

Local structure of condensed zinc oxide

F. Decremps,* F. Datchi, A. M. Saitta, and A. Polian

Physique des Milieux Condensés, CNRS-UMR 7602, Université Pierre et Marie Curie, Tour 13, B77, 4, place Jussieu, 75252 Paris CEDEX 05, France

S. Pascarelli

European Synchrotron Facility, BP 220, 38043 Grenoble, France

A. Di Cicco

INFN, Dipartimento di Matematica e Fisica, Università di Camerino, via Madonna delle Carceri, 62032 Camerino (MC), Italy

J. P. Itié and F. Baudelet

Physique des Milieux Condensés, CNRS-UMR 7602, Université Pierre et Marie Curie, B77, 4, place Jussieu, 75252 Paris CEDEX 05, France

(Received 8 January 2003; revised manuscript received 2 May 2003; published 2 September 2003)

The high-pressure local structure of zinc oxide has been studied at room temperature using combined energy-dispersive x-ray-diffraction and x-ray-absorption spectroscopy experiments. The structural parameter u and the lattice-parameter ratio c/a of the wurtzite phase is given as a function of pressure and compared with results from *ab initio* calculations based on a plane-wave pseudopotential method within the density-functional theory. It is shown that an accurate study of ZnO requires the explicit treatment of the d electrons of Zn as valence electrons. In good agreement with present calculations, our experimental data do not show any variation of $u(P)$ in the low-pressure wurtzite phase between 0 and 9 GPa, pressure at which the phase transition to the rocksalt phase occurs. Moreover, no dramatic modification of the r -phase K -edge position up to ~ 20 GPa is observed, indicating the absence of metallization. In view of all these results, theoretical models identifying the wurtzite-to-rocksalt transition as an homogeneous path are discussed.

DOI: 10.1103/PhysRevB.68.104101

PACS number(s): 61.10.Ht, 62.50.+p, 61.50.Ks

I. INTRODUCTION

Aside from being a good sunblock to protect the skin from UV overexposure, ZnO is a transparent piezoelectric semiconductor which occurs naturally as a mineral (called zincite), e.g., at the meeting point of three relevant groups for physics, materials science, and geophysics. More specifically, high-pressure experimental data on this compound are fundamental to condensed-matter physics because they constrain empirical models of the interatomic potential repulsive part in semiconductors, which might afterwards benefit the design of optoelectronic devices.

As pressure is raised from an ambient condition, ZnO and group-III nitrides (AlN, GaN, and InN) transform from fourfold (wurtzite, labeled w ; $P6_3mc$ space group) to sixfold (rocksalt, labeled r ; $Fm\bar{3}m$ space group) coordinated crystal structures. The microscopic mechanism involved in this transformation has been the subject of numerous studies and the existence of a transition path is still debated. Recent theoretical calculations of phonon dispersion have shown that standard total-energy calculations might lead to wrong conclusions regarding the occurrence of high-pressure structural phase transitions.^{1,2} Moreover, lattice-dynamical properties are helpful for understanding the transformation pathways. For example, w -InN was predicted³ to be unstable prior to the transition to the r -high-pressure phase, leading to a second-order isostructural transformation from the standard wurtzite phase to another hexagonal configuration (labeled w'). Recently, Serrano *et al.*⁴ refined the previous conclu-

sion using density-functional theory (DFT) local-density approximation (LDA) calculations and found a clear variation of the internal crystallographic parameter u from its ambient value ($\sim \frac{3}{8}$) up to 0.5 when w -AlN and w -InN are pressurized. The same type of intermediate phase transformation has been described for GaN,⁵ where, via a group-theory analysis of the group-subgroup relationship between the two wurtzite networks, a transformation involving coherent atomic motions rather than a simple unpredictable diffusion is proposed. However, this result has been confirmed neither experimentally nor theoretically.⁶ This behavior has only been calculated for group-III nitrides and the presence of such transformation in ZnO is probed and discussed in the present paper (Sec. IV).

The variation of u up to 0.5 has never been observed experimentally, probably because the w -to- w' transformation is usually predicted to occur at a pressure above the observed first-order w -to- r transition. Nevertheless, if such phase transition exists in nitrides or ZnO, it should be preceded by some structural instabilities in the w phase, such as a nonlinear pressure behavior of c/a and u ³ or phonons softening.⁵ Experimentally, the elastic behavior of ZnO has been determined by ultrasonic experiments up to the w -to- r transition pressure (9 GPa). An unusual negative value for the shear modes has been observed and indicates that w -ZnO is indeed unstable with respect to a shear perturbation,⁷ a result that has been recently confirmed by theory.⁸ By contrast, no anomalous behavior is seen for any optical mode in the experiments or calculations.⁹ Thus, an accurate measurement of

$u(P)$ in ZnO would shed some light on the w -structure stability. In addition, the determination of the bond distance Zn-O as a function of pressure is the most direct way to explore the repulsive part of the interatomic potential, which is of great importance for the understanding of ZnO physical and chemical properties.

The room-temperature compression behavior of w - and r -ZnO was studied previously by x-ray powder diffraction.^{10–15} However, neither calculations nor experiment regarding the pressure dependence of the local structure of w -ZnO has been published. An experimental attempt to determine $u(P)$ has been proposed¹¹ by comparing the integrated intensity of the (002) and (101) energy-dispersive x-ray-diffraction lines. But, according to the author, in view of the problems arising from the extraction of the powder quality (texture, microstrain, orientation) and the pattern background contributions (Compton scattering, fluorescence), more work is needed to obtain reliable data on the local structure. Results from high-pressure ⁶⁷Zn-Mössbauer spectroscopy on w -ZnO allowed to probe the hyperfine interactions related to the valence state of zinc.¹³ But, here again, the pressure variation of the microscopic structure can only be deduced indirectly [through the use of lattice dynamics and linearized augmented plane-wave (LAPW) band-structure calculations].

The principal objective of this study is to achieve atomic-scale insight into the wurtzite structure stability of condensed ZnO. The pressure variation of the atomic positions in both wurtzite and rocksalt phases are first calculated through the density-functional perturbation theory approach using a standard local-density approximation plane-wave/pseudopotential scheme, and, secondly, probed experimentally by Zn extended x-ray-absorption fine-structure (EXAFS) calculations. It is well known that EXAFS analysis suffers from the ambiguity that the results are strongly dependent on the number of fitting parameters.¹⁶ This is particularly critical in the case of the wurtzite structure where, at least, contributions up to the fifth shell including multiple-scattering effects have to be taken into account to satisfactorily refine the experimental x-ray-absorption fine-structure (XAFS) spectra. Thus, at the same experimental conditions of pressure, temperature, powder texture, and strain state, x-ray diffraction (XRD) patterns were recorded to follow the long-range order. The present x-ray-absorption spectroscopy (XAS) and XRD combined study allows to confirm the reliability of our analysis by checking the pressure dependence of $a(P)$ and $c(P)$ deduced from XAFS,¹⁷ against that obtained independently from XRD data treatment.

In addition, high-pressure x-ray-absorption near-edge structure (XANES) measurements of bulk ZnO were carried out in order to get an accurate determination of the Zn K -edge pressure dependence. Up to ~ 20 GPa, no dramatic modification of the r -phase edge position indicates the absence of metallization. Further, the structures of both w - and r -ZnO under pressure have been confirmed by comparing the XANES raw data with full multiple-scattering calculations. In particular, the present study allows to disentangle the ambiguity of the crystallographic structure of the recovered sample at $P=0$. Finally, the experimental results are com-

pared with original results from *ab initio* calculations and discussed in terms of wurtzite stability and the microscopic w -to- r transition process.

II. EXPERIMENTS

A. Sample and high-pressure apparatus

The high-pressure cell was a conventional membrane diamond-anvil cell.¹⁸ A steel gasket was preindented from 200 to 60 μm , and a 150- μm hole was drilled in the center by spark erosion. Polycrystalline zinc oxide with a nominal purity of 99.9995%, purchased from Alfa AESAR, was loaded into the gasket hole. Chemically inert, silicon oil was used as a pressure transmitting medium. Pressure was systematically measured *in situ* before and after each measurement using the fluorescence emission of a ruby ball^{19,20} placed into the gasket hole. The accuracy was better than 0.5 GPa at the maximum pressure reached.

B. X-ray diffraction

X-ray-diffraction experiments were performed at Laboratoire pour l'Utilisation du Rayonnement Electromagnetique (LURE) (Orsay, France), where the synchrotron radiation is emitted by the DCI storage ring operating at 1.85 GeV with typical currents of 300 mA. The powder x-ray-diffraction measurements were made in the energy-dispersive mode with the wiggler at the DW11 station. After the energy calibration of the Ge detector, the 2θ angle was determined by collecting diffraction patterns of a gold sample placed in between the anvils ($2\theta=13.759^\circ$). The polychromatic x-ray beam was collimated to a $50\times 50\text{-}\mu\text{m}^2$ spot centered on the gasket hole and the diffraction patterns were collected for up to 600 s.

C. Extended x-ray-absorption fine structure

Extended x-ray-absorption fine-structure spectroscopy was performed at LURE, at the D11 dispersive XAS station at the Zn K edge. The calibration of the photon energy scale was determined comparing the K -edge pure Zn spectrum collected at ambient conditions using the dispersive technique with analogous spectra recorded with the same conditions using the standard XAS technique (double-crystal scanning monochromator). The position of the diamond cell was optimized in order to reject strong Bragg peaks from the diamonds at high energy above the absorption edge: the available energy range was up to about 500 eV above the Zn K edge. Additional details of the beamline setup and the procedure of pattern acquisition have been previously published.²¹

D. X-ray-absorption near-edge structure

The high-pressure Zn K -edge XANES measurements on bulk ZnO were carried out at the European Synchrotron Radiation Facility on beamline ID24.²² A curved Si(111) crystal polychromator horizontally focused a $\sim 500\text{-eV}$ fan of radiation onto a $\sim 30\text{-}\mu\text{m}$ spot. A Pt-coated mirror, placed $\sim 60\text{-cm}$ upstream of the sample at a grazing incidence angle of 4 Mrad, was used to vertically refocus the beam down to below 30- μm full width at half maximum.²³

E. Computer experiment: Method of calculation

The high-pressure structural properties of zinc oxide have also been studied by means of *ab initio* computer simulations. Our calculations have been performed using the PWSCF code,²⁴ and are based on the DFT within the local-density approximation.¹ A standard plane-wave/pseudopotential scheme is adopted. Our pseudopotentials are chosen through the Troullier-Martins scheme.²⁵ Other zinc-based semiconductors can accurately be treated by freezing the zinc *d* electrons in the core, and adopting a nonlinear core-correction scheme to account for this approximation. An accurate study of ZnO requires instead the explicit treatment of the *d* electrons of Zn as valence electrons. This choice, although computationally demanding, proves essential in yielding, for example, the correct energetics of the different structures. Our calculations were performed with a kinetic-energy cutoff of 75 Ry, and special *k*-points integration in the Brillouin zone, with (444) or (666) regular grids.

The wurtzite structure contains two parameters not fixed by symmetry, i.e., the *c/a* ratio and the internal coordinate *u*. In order to determine the pressure behavior of the system in the wurtzite phase, we chose to fix different volumes, and to relax the total energy of the crystal with respect to those parameters. This method allows us to obtain an energy-volume equation of state which can be fitted with a Murnaghan equation. The same kind of calculation is straightforwardly performed in the cubic NaCl phase, where of course the only variable is the lattice parameter.

III. ANALYSIS

A. X-ray-diffraction data

The x-ray-diffraction data were analyzed using DATLAB software.²⁶ Figure 1 shows a stack of *w*- and *r*-ZnO XRD spectra recorded from ambient to high pressure where the background has been subtracted. Because the origin of the background is multiple (synchrotron source, detector, and absorption of the sample and its environment) and difficult to quantify, it was fitted to a polynomial function up to third order. Peak positions were determined using a pseudo-Voigt model and the lattice spacings d_{hkl} (in Å) were extracted from the energies of the reflection lines E_{hkl} (in keV) using Bragg's law: $E_{hkl} \cdot d_{hkl} = 6.199/(\sin \theta)$. Finally, the lattice parameters were calculated using a classical least-squares refinement program. The relative errors of the lattice parameters were determined to be less than 0.05% in all refinements.

B. EXAFS

EXAFS data analysis was carried out in the framework of the GNXAS codes²⁷⁻²⁹ for theoretical calculations of x-ray-absorption fine structure including multiple-scattering (MS) pathways. The simulations were performed using the muffin-tin approximation and the Hedin-Lundqvist exchange-correlation self-energy. The refinement is based on a minimization of a standard χ^2 -like residual function related to the difference between the raw experimental absorption coefficient and the theoretical signal.³⁰ Using continued-fraction

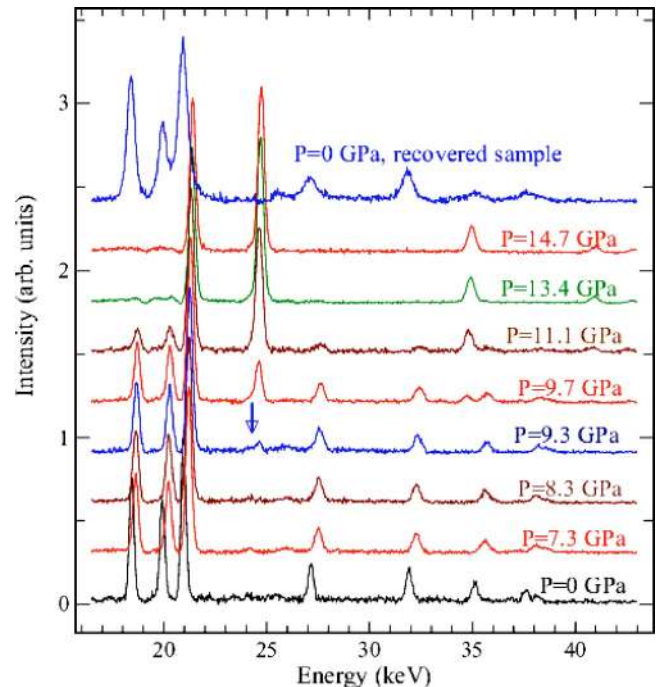


FIG. 1. X-ray energy-dispersive spectra for wurtzite and rock-salt ZnO at different pressures. At 9.3 GPa, a new diffraction peak (arrow) reflects the occurrence of the *w*-to-*r* phase transition. On decompression (from 16 GPa), the diffraction pattern fingerprint of the *w* phase reappears at ~ 2 GPa.

techniques, the XAFS signal calculations were performed including both two-atom and three-atom irreducible MS terms [respectively, noted $\gamma^{(2)}$ and $\gamma^{(3)}$].²⁷ In the following, using standard notation, the *n*-body distribution function peaks of the *i*th shell are labeled $g_i^{(n)}$. Before fitting the experimental signal with a theoretical model, a preanalysis was performed in order to (i) simulate the atomic background, including the main anomalies due to the opening of double-electron excitation channels; (ii) determine for each structure the relevant fitting process.

1. Background subtraction

The presence of double-electron photoexcitations, even tiny, usually results in anomalies in the EXAFS signal background which affect the reliability of the local structure determination (see, for example, Appendix A2 of Ref. 29). The study of double-electron excitations in the Zn *K* edge has only been attempted in the vicinity of the *K* edge.³¹ At highest energy (where the double-electron photoexcitations may create anomalies in the EXAFS signal), more relevant results have only been obtained with copper³² and 4*p* elements from $Z=31$ (Ga) to $Z=36$ (Kr),³³ where the magnitude of the opening of absorption channels creating the $[1s3p]$ and $[1s3d]$ double-hole configurations is shown to linearly increase with decreasing *Z*. The presence of these channels has also been evidenced for Ga and Ge ($Z=32$), whose contribution appears to be absolutely necessary for reasonable EXAFS fits.²⁸ Moreover, the amplitude of the $[1s3p]$ double-electron excitation cross section has been experimen-

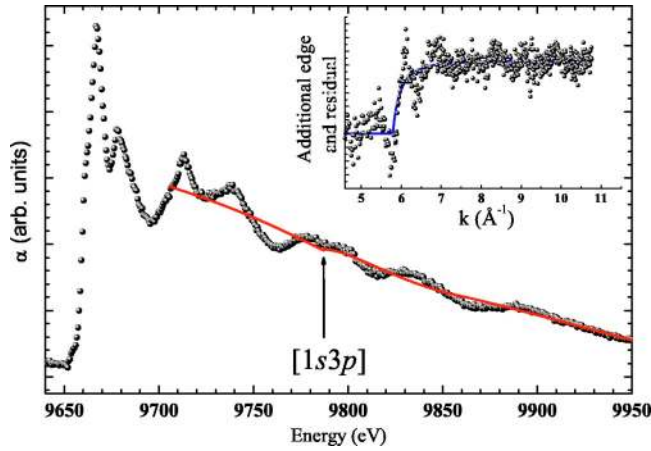


FIG. 2. Raw K -edge spectrum of w -ZnO at $P=0$ and background (modeled using a four degree polynomial function) with visible double-electron excitation at ~ 9790 eV. Inset: magnified plot of double-electron excitation shape (line) and residual experimental signal. The background parameters were independently refined for each spectra (different pressure, different structure), and no significant difference was detected. It indicates, in particular, the expected transferability of double-electron features from one structure (w) to another (r).

tally shown to be larger when the metal is oxydized (mainly due to the more efficient $1s$ hole screening in metal than in its corresponding oxide³⁴). Thus, the extrapolation of previous results to $Z=30$ (Zn) justifies the background correction procedure used in the present work on ZnO, where the $[1s3p]$ double-electron feature has been taken into account. Experimental EXAFS spectra of w -ZnO at ambient conditions and a best-fit model background including double-electron features are reported in Fig. 2. The empirical background anomaly has been fitted to the experimental data using the “smooth step” function available in the FITHEO program of GNXAS.²⁹ As empirically expected, the amplitude of the $[1s3p]$ cross section is significant. Its energy can be roughly estimated using the $Z+1$ rule leading in the case of Zn to 100 eV ($3p_{3/2}$) and 103.5 eV ($3p_{1/2}$) above the main $1s$ edge. It can be noted that these values are slightly lower than the $[1s3p]$ energy observed in this work (~ 9790 eV), probably because of a merging between $[1s3s]$ and $[1s3p]$ contributions.

2. Wurtzite phase analysis

Using the GNXAS code, an initial study revealed that whereas a substantial contribution to the EXAFS signal is given by the oxygen nearest neighbors, the additional contributions from the next-nearest neighbors are essential to account for the total EXAFS signal. However, increasing the number of fitting parameters dramatically decreases the accuracy of the result and a strategy has to be developed to choose appropriate fitting parameters and to find connections between them.

It is obvious that in a general triangular three-atom configuration, the structural parameters R_{12} , R_{13} , and θ_{213} automatically define the third interatomic distance R_{23} (see Fig.

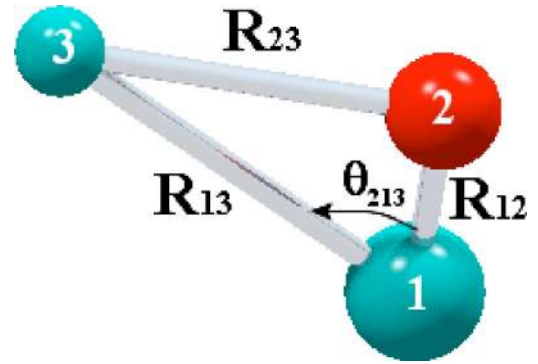


FIG. 3. Schematic representation of a three-body configuration. The corresponding EXAFS signal is specified by the parameters R_{12} , R_{13} , and θ_{213} , the third distance R_{23} being calculated through the Carnot formula.

3). Therefore, the doublet $\gamma^{(2)}$ signals beyond the second shell can be calculated using the corresponding triplet coordinates. This strategy avoids the use of further structural parameters by introducing in the fitting process an interconnection between the $g^{(2)}$ and the $g^{(3)}$ peaks through the Carnot formula.³⁵ In the following, the two-atom signals $\gamma^{(2)}$ of the second shell [$g_2^{(2)}$ peak] and the fourth shell [$g_4^{(2)}$ peak] are calculated using the three-atom contributions $\gamma^{(3)}$ [$g_1^{(3)}$ and $g_3^{(3)}$ peaks, respectively]. A single effective multiple-scattering signal $\eta^{(3)}$ including both the $\gamma^{(2)}$ and the $\gamma^{(3)}$ contributions is used for the corresponding shells.

All XAFS signals $\gamma^{(n)}$ reported in Table I have been calculated up to 1000 eV above the Zn K edge and considered for reproducing the experimental XAFS spectra collected under pressure. In addition to the background, the XAFS calculated signal has been refined using a total number of two empirical parameters (E_0 , defining the alignment of the energy scale, and S_0^2 , rescaling the calculated EXAFS signal) and ten structural parameters: the six parameters describing the three two-body distributions (distance R and corresponding variance σ_R^2 for each doublet) and the four parameters

TABLE I. Pair and triplet configurations for w -ZnO at ambient conditions. The three coordinates defining the three-body peaks are as described in Fig. 3. The degeneracy is specified for each configuration.

Peak	R_{12} (Å)	R_{13} (Å)	θ_{213} (°)	Degeneracy	Atoms	XAFS signal
$g^{(2)}$						
1	1.977			4	Zn-O	$\gamma_1^{(2)}$
2	3.207			6	Zn-Zn	$\gamma_2^{(2)}$
3	3.214			1	Zn-O	$\gamma_3^{(2)}$
4	3.250			6	Zn-Zn	$\gamma_4^{(2)}$
5	3.807			9	Zn-O	$\gamma_5^{(2)}$
$g^{(3)}$						
1	1.977	1.977	108.11	6	O-Zn-Zn	$\gamma_1^{(3)}$
2	1.977	1.977	108.11	3	Zn-O-O	$\gamma_2^{(3)}$
3	1.977	1.977	110.80	6	O-Zn-Zn	$\gamma_3^{(3)}$

TABLE II. Pair and triplet configurations for *r*-ZnO at ambient conditions. The three coordinates defining the three-body peaks are as described in Fig. 3. The degeneracy is specified for each configuration.

Peak	R_{12} (Å)	R_{13} (Å)	θ_{213} (°)	Degeneracy	Atoms	XAFS signal
$g^{(2)}$						
1	2.142			6	Zn-O	$\gamma_1^{(2)}$
2	3.029			12	Zn-Zn	$\gamma_2^{(2)}$
3	3.710			8	Zn-O	$\gamma_3^{(2)}$
4	4.284			6	Zn-Zn	$\gamma_4^{(2)}$
$g^{(3)}$						
1	2.142	2.142	90.0	24	O-Zn-Zn	$\gamma_1^{(3)}$
2	12.142	2.142	90.0	12	Zn-O-O	$\gamma_2^{(3)}$
3	2.142	2.142	180.0	6	O-Zn-Zn	$\gamma_3^{(3)}$

describing the two three-body distributions (angle mean value θ and corresponding variance σ_θ^2). The coordination numbers have been kept unchanged under pressure. The decomposition of the best-fit multiple-scattering signal into individual $\gamma^{(2)}$ and $\eta^{(3)}$ terms is shown in Fig. 4. In all refinements, the value of the amplitude reduction factor S_0^2 has been found to lie around 0.95(5) and E_0 was found to coincide within 1 eV with the energy position of the second peak of the experimental spectra derivative (9663 eV).

3. Rocksalt phase analysis

All XAFS signals $\gamma^{(n)}$ reported in Table II have been calculated up to 1000 eV above the Zn *K* edge and considered for reproducing the experimental XAFS spectra collected under pressure. The signal has been modeled as a sum of five contributions described as follows (the corresponding structural parameters are listed in brackets): (i) First shell Zn-O $\gamma_1^{(2)}$ ($R_1, \sigma_{R_1}^2$); (ii) three-body O-Zn-Zn contribution $\eta_1^{(3)}$ associated with the $\theta_1=90^\circ$ triangles where the long bond coincides with peak two of the $g^{(2)}$ ($R_1, \sigma_{R_1}^2, \theta_1, \sigma_{\theta_1}^2$; the other covariance matrix parameters are fixed as for the *w*-ZnO XAFS analysis); (iii) third shell Zn-O $\gamma_3^{(2)}$ ($R_3, \sigma_{R_3}^2$); (iv) three-body O-Zn-Zn contribution $\eta_1^{(3)}$ associated with the $\theta_1=180^\circ$ triangles where the long bond coincides with peak four of the $g^{(2)}$ ($R_1, \sigma_{R_1}^2, \theta_1, \sigma_{\theta_1}^2$); (v) three-body Zn-O-O contribution $\gamma_2^{(3)}$ associated with the $\theta_1=90^\circ$ triangles ($R_1, \theta_1, \sigma_{\theta_1}^2$). The empirical parameters E_0 (~ 9664 eV) and S_0^2 (~ 0.90) have been fitted together with the structural parameters and the best-fit XAFS signal is shown in Fig. 5.

C. XANES

From a qualitative point of view, x-ray-absorption near-edge spectroscopy (XANES) is one of the most sensitive techniques for probing pressure-induced structural modifications. Figure 6 shows raw Zn *K*-edge XANES data recorded as a function of pressure during the upstroke ramp, up to *P*

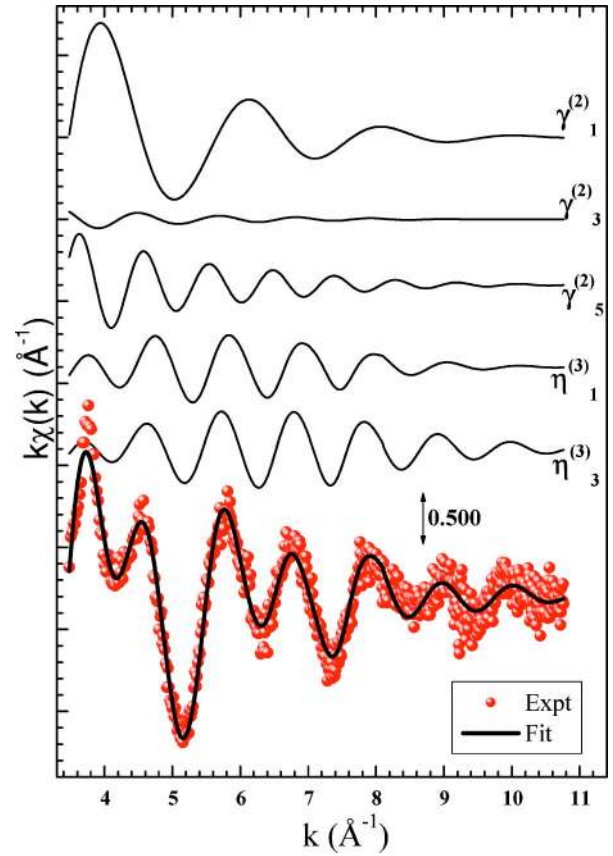


FIG. 4. Best-fit calculated multiple-scattering signals for the Zn *K*-edge XAFS $k\chi(k)$ spectra of *w*-ZnO recorded at ambient pressure. The $\gamma_1^{(2)}$, $\gamma_3^{(2)}$, and $\gamma_5^{(2)}$ signals are associated with the first, third, and fifth shell of neighbors, respectively. The two triplet signals are indicated as $\eta_1^{(3)}$ and $\eta_3^{(3)}$ because they include also the doublet associated with the longest interatomic distance of the triangle [$\gamma_2^{(2)}$ and $\gamma_4^{(2)}$, respectively]. Note the absence of the $\gamma_2^{(3)}$ signal because (i) its amplitude has been found to be too weak to be taken into account and (ii) the longest distance of the corresponding atoms triplet does not involve the photoabsorbing atom (Zn). The agreement between measured (Expt) and calculated (Fit) spectra is excellent in the whole energy range.

~ 16 GPa. In good agreement with XRD or EXAFS, the data shows the onset of a phase transition to the NaCl phase around 10 GPa, the transition being complete at about 14 GPa.

In principle, a complete recovery of the local geometry and site coordination around Zn could be obtained from XANES. However, the quantitative analysis of this region presents difficulties mainly related to the theoretical approximation in the treatment of the potential and the need for heavy time-consuming algorithms to calculate the absorption cross section in the framework of a full multiple-scattering approach. We have performed a comparison of the data with full multiple-scattering calculations using a self-consistent energy-dependent exchange-correlation Hedin-Lundqvist potential (FEFF8 package³⁶). Self-consistency was obtained by successively calculating the electron density of states, electron density, and Fermi level at each stage of the calculation within a 27-atom cluster (4 Å or \sim three shells) centered on

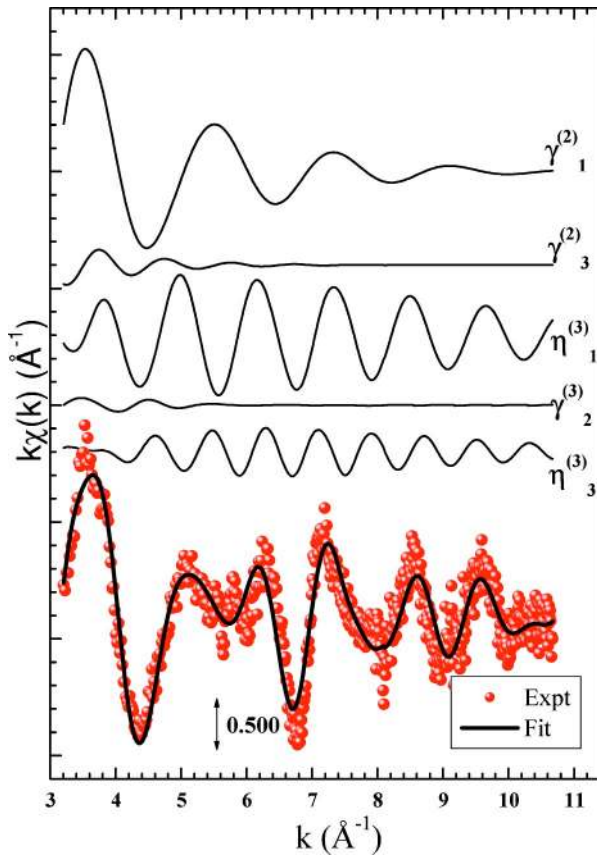


FIG. 5. Best-fit calculated multiple-scattering signals for the Zn K -edge XAFS $k\chi(k)$ spectra of r -ZnO recorded at ambient pressure. Here again, the agreement between measured (Expt) and calculated (Fit) spectra is excellent.

the atom for which the density of states is calculated, and then iterated. Full multiple-scattering XANES calculations were carried out for a 93-atom cluster (6.2 Å or \sim seven shells) centered on the absorbing atom: all multiple-scattering paths within this cluster were summed to infinite order. Besides the structural information defining the geometry of the cluster ($a=3.2427$ Å, $c=5.1948$ Å, and $u=0.3826$ for w -ZnO; $a=4.280$ Å for r -ZnO), the only external parameters used as input for the XANES simulations were a 0.5-eV experimental broadening, and a small offset in the energy scale (-5.0 eV). A typical result of the simulations for the wurtzite and NaCl phases of bulk ZnO are shown in Fig. 7. The overall good agreement between the calculated and the measured spectra is striking, considering the absence of adjustable parameters in the theory (in particular, no structural disorder factor was added to the simulations). The major features and their variation with pressure are correctly reproduced.

IV. RESULTS AND DISCUSSION

A. Wurtzite phase

The structures of both w - and r -ZnO under pressure have been confirmed by comparing the XANES raw data with full

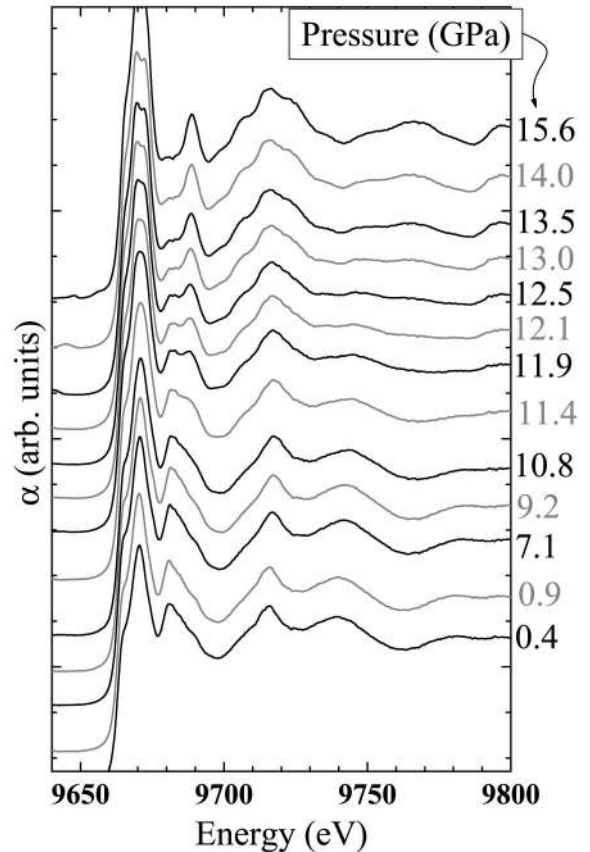


FIG. 6. Zn K -edge XANES spectrum of bulk ZnO as a function of pressure during the upstroke ramp.

multiple-scattering calculations. In particular, the present study dispels the ambiguity of the crystallographic structure of the recovered sample at $P=0$ which is found to be pure wurtzite.

Within the approximation described in Ref. 17, the EXAFS analysis was sophisticated enough to determine both internal (u) and unit-cell (c , a) parameters as a function of pressure. As a matter of fact, the wurtzite symmetry sets the relation between u , c , a , and the $g_i^{(n)}$ peaks position (see Table III).

The EXAFS results $a(P)$, $c(P)$, and $V(P)$ are plotted in Fig. 8 with both experimental x-ray diffraction and *ab initio* results for comparison. Cell-parameter [$l(P)$] measurement as a function of pressure was analyzed with the Murnaghan equation of state: $l(P)=l(0)\cdot[1+(B'/B_0)\cdot P]^{(-1/B')}$, where B' is the pressure derivative of the isothermal incompressibility at 300-K B_0 (results summarized in Table IV). A linear fit to the data gives $d(c/a)/dP=-0.0004$ GPa $^{-1}$, in excellent agreement with previous work.¹¹ The EXAFS results of $d_{Zn-O}(P)$ and $u(P)=d_{Zn-O}(P)/c(P)$ are given in Fig. 9.

The variation of d_{Zn-O} has been fitted with the Murnaghan equation of state, leading to $B_{d0}=420$ GPa [with $d_{Zn-O}(0)=1.985$ Å and B'_d fixed to 12]. In good agreement with Desgreniers,¹¹ the u oxygen positional parameter indi-

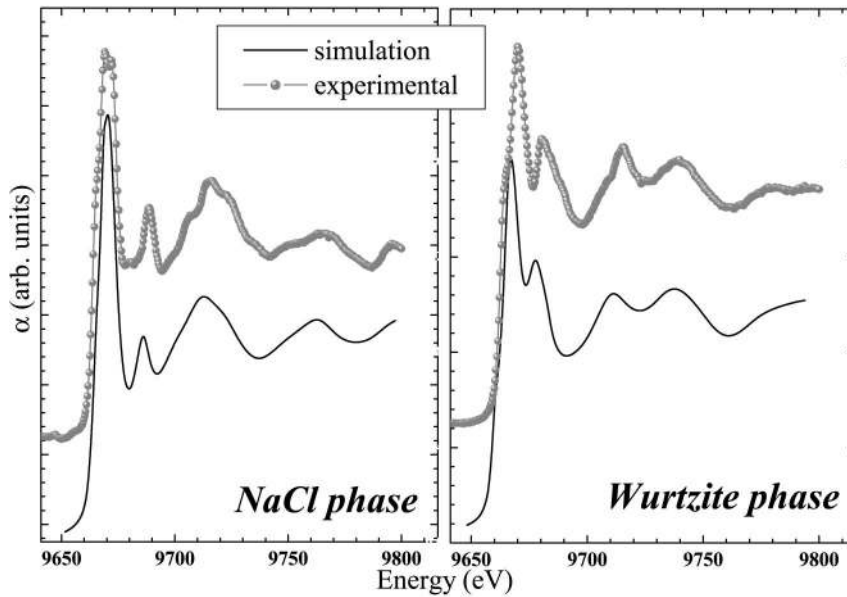


FIG. 7. Left: Zn K -edge XANES of bulk r -ZnO at $P = 15.6$ GPa and *ab initio* simulated spectrum for the NaCl phase. Right: Zn K -edge XANES of bulk w -ZnO at $P = 0.4$ GPa and *ab initio* simulated spectrum for the wurtzite phase.

cates, within experimental uncertainty, no peculiar change under pressure.⁴⁰ Karzel *et al.*¹³ predicted an increase of u to explain their ^{67}Zn -Mössbauer spectroscopy results (pressure dependence of the main component V_{zz} of the electric-field gradient tensor). However, this discrepancy with our result can stem from the fact that the $V_{zz} \leftrightarrow u$ correlation has been indirectly deduced from scalar-relativistic linearized-augmented plane-wave (LAPW) calculations, V_{zz} being measured at low temperature (4.2 K).

B. Rocksalt phase

The present XRD and EXAFS high-pressure experiments show the occurrence of a phase transition from the wurtzite to the rocksalt phase at about 9 GPa (kinetic pressure transition). Theoretically, the rocksalt structure is seen to be more stable against the wurtzite one at pressure higher than 7.6 GPa, in good agreement with the experimental thermodynamic equilibrium transition observed at around 6 GPa.¹⁵ The experimental (EXAFS, XRD) and theoretical results of $V(P)$ for the r phase are given in Fig. 10.

The pressure dependence of V (cell volume per chemical formula) has been fitted for decreasing pressure between 20 and 2 GPa with the Birch-Murnaghan equation of state.

TABLE III. Two- and three-body distribution function peaks and associated interatomic distances as a function of internal (u) and unit-cell (c , a) parameters of the wurtzite structure. The long-bond distance of the triplet peaks corresponds to the distance R_{23} of Fig. 3.

Peaks	Atoms	Distances	Long-bond distances
$g_1^{(2)}$	Zn-O	$u \cdot c$	
$g_3^{(2)}$	Zn-O	$(1-u) \cdot c$	
$g_5^{(2)}$	Zn-O	$\sqrt{a^2 + c^2} \cdot u^2$	
$g_2^{(3)}$	O-Zn-Zn		$\sqrt{a^2/3 + c^2/4}$
$g_3^{(3)}$	O-Zn-Zn		a

Given in Table V, the present results obtained from both experimental and theoretical studies are in excellent agreement with previously reported data.^{10–14,37,39}

It can be noted that in other II-VI compounds, the transition of the low-pressure to rocksalt high-pressure phase is usually associated with a metallization. In the case of ZnO,

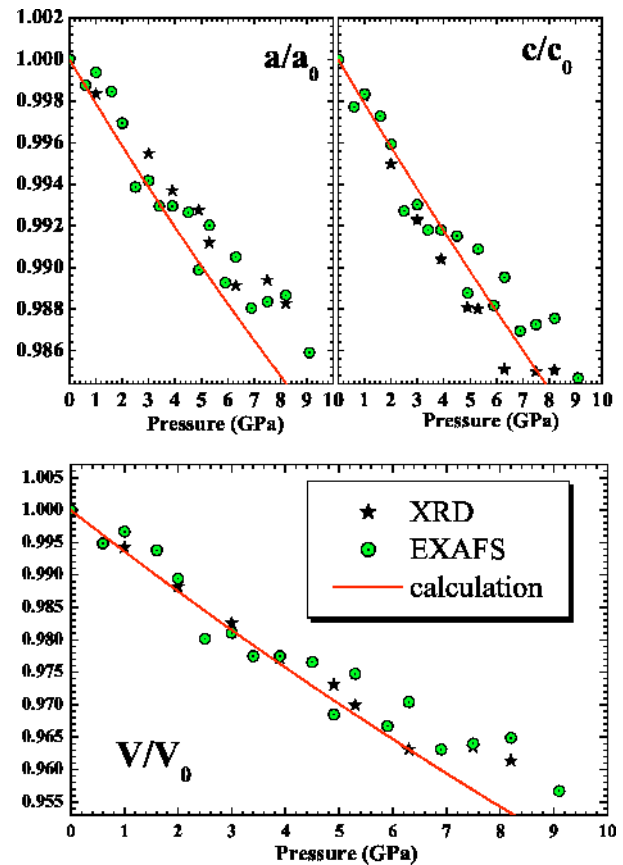


FIG. 8. Pressure dependence of the cell parameters for the wurtzite phase among compression.

TABLE IV. Murnaghan equation-of-state parameters for the wurtzite phase of ZnO. Generalized gradient approximation is represented as GGA. Superscripts *F* indicate a fixed value of *B'* in the Murnaghan fitting. Volumes *V*, in Å³, are per chemical formula unit. Distances *a* and *c* are in Å. Isothermal bulk moduli are in GPa. *B*_{*i0*} defines the linear incompressibility along the *i* axis, with *B*'_{*i*} its pressure derivative.

References	Method	<i>a</i> ₀	<i>B</i> _{<i>a0</i>}	<i>B</i> ' _{<i>a</i>}	<i>c</i> ₀	<i>B</i> _{<i>c0</i>}	<i>B</i> ' _{<i>c</i>}	<i>u</i> ₀	<i>V</i> ₀	<i>B</i> ₀	<i>B</i> '
This work	XRD	3.250	614	12 ^{<i>F</i>}	5.201	406	12 ^{<i>F</i>}		23.79	173	4 ^{<i>F</i>}
This work	EXAFS	3.258	564	12 ^{<i>F</i>}	5.220	491	12 ^{<i>F</i>}	0.382	23.99	181	4 ^{<i>F</i>}
This work	DFT-LDA	3.238	464	15	5.232	466	9	0.380	23.76	154	4.3
11	X ray	3.2498			5.2066				23.810	142.6	3.6 ^{<i>F</i>}
13	XRD+Mössbauer	3.2496			5.2042				23.796	183	4 ^{<i>F</i>}
14	XRD	3.2475			5.2075				23.7847	136	9.4
37	LDA							0.379	22.874	162.3	4.05
37	GGA							0.3802	24.834	133.7	3.83
39	Hartree-Fock							0.3856	24.570	154.4	3.6
13	LAPW							0.381		160	4.4

the present XANES analysis shows the *K*-edge energy position to increase at the *w*-to-*r* transition, indicating an increase of the band gap. Further, no dramatic modification of the *r*-phase edge position up to ~20 GPa is observed, indicating the absence of metallization, in agreement with reported conductivity measurements.³⁸

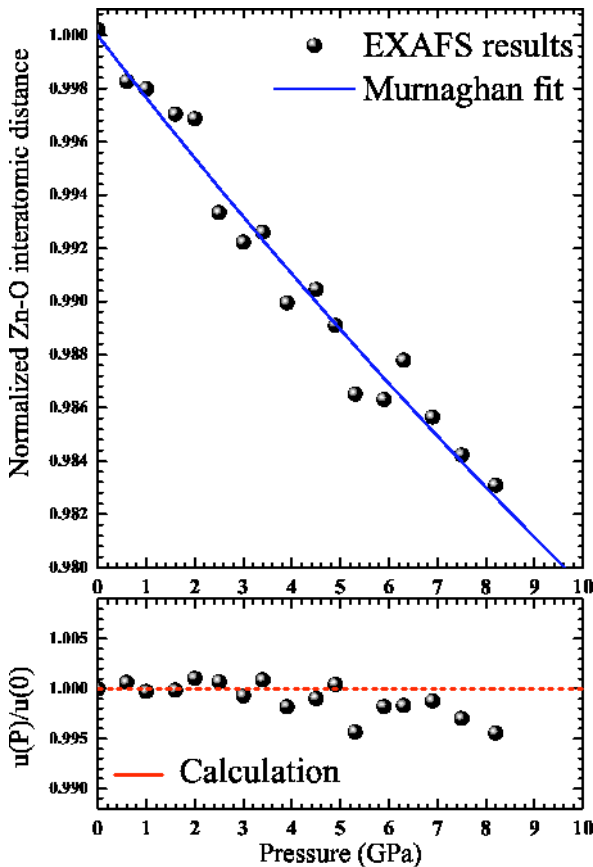


FIG. 9. Pressure dependence of the first-nearest-neighbors distance of zinc (*d*_{Zn-O}) and the internal cell parameter (*u*) for the wurtzite phase.

C. Transition path

As recalled in the Introduction, a transition path between the *w* and the *r* phase has been proposed in the literature involving the occurrence of an intermediate hexagonal phase, labeled *w'*. It is clear that no such phase is observed experimentally and that the *w* phase is transformed directly into the *r* phase above 9 GPa at 300 K. However, it is interesting to probe the respective stability of the *w* and *w'* phases, which can be done theoretically above the *w*-to-*r* experimental transition pressure.

In Fig. 11 we report the total energy vs the *c/a* ratio along three isochores of *w*-ZnO. The corresponding values of pressure, in the wurtzite range (i.e., for *c/a* ≈ 1.6), are about 19, 29, and 39 GPa. These calculations show the existence of a second minimum around *c/a* ≈ 1.28, which corresponds to the *w'* phase. This structure is metastable at any pressure, and becomes more stable than the *w* phase beyond 20 GPa. However, a phase transition between those two structures would still be discontinuous at pressures below about 40 GPa. In fact, as shown in the figure, there is an energy barrier along this transformation path up to 39 GPa. Consequently, a

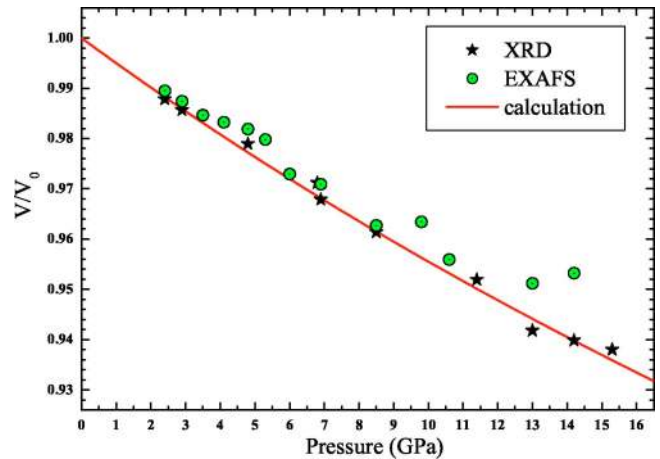


FIG. 10. Pressure dependence of the cell volume for the rocksalt phase (upon decompression for experimental data).

TABLE V. Murnaghan equation-of-state parameters for the rocksalt phase of ZnO. Superscripts F indicate a fixed value of B' in the Murnaghan fitting. Volumes V , in \AA^3 , are per chemical formula unit. Isothermal bulk moduli are in GPa. The EXAFS results have been obtained through the d_{Zn-O} measurements using the cubic symmetry relation $d_{Zn-O} = a/2 = (V/2)^{1/3}$.

Method	V_0	B_0	B'
XRD	19.64	204	4^F
EXAFS	19.70	218	4^F
DFT-LDA	19.49	198	4.6

kink in the pressure variation of u is observed at 24 GPa, pressure higher than the experimental w -to- r pressure transition. The change of the u value from 0.382 (initial low-pressure value) up to 0.5 is obviously connected to a symmetry change of the structure which can be seen as an intermediate phase (w') between w - and r -ZnO.⁵ As a matter of fact, this interpretation is of most interest, since in view of the P - T phase diagram of ZnO,¹⁵ the w -to- w' transformation could be observable at low temperature, a domain in which the pressure stability range of the w phase is expected to be larger (against the rocksalt phase) than at 300 K.

However, in opposition with previous predictions^{3,5} of an homogeneous path along which w -ZnO is *continuously* transformed to r -ZnO, the present calculations lead to a constant value of u below and above 24 GPa, pressure at which an abrupt *discontinuity* from 0.382 to 0.5 is observed. In the mean time, experimental data do not show instability of the wurtzite structure which could be expected below the w -to- w' transition. The present EXAFS analysis gives a pressure-independent value of u in the wurtzite stability range. From the XANES analysis, the structural phase transition is shown (Fig. 12) to induce modifications in the electronic structure that lead to an energy shift of about +1 eV in the onset of absorption (defined as the energy corresponding to the maximum of the first derivative at the absorption edge). However, the Zn K -edge energy for the wurtzite phase is unchanged

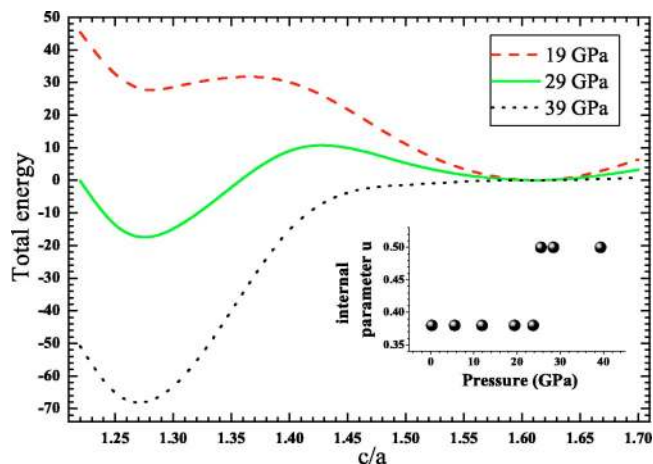


FIG. 11. Total energy of the wurtzite crystal with respect to the c/a ratio. Inset: Calculated pressure dependence of the internal parameter u .

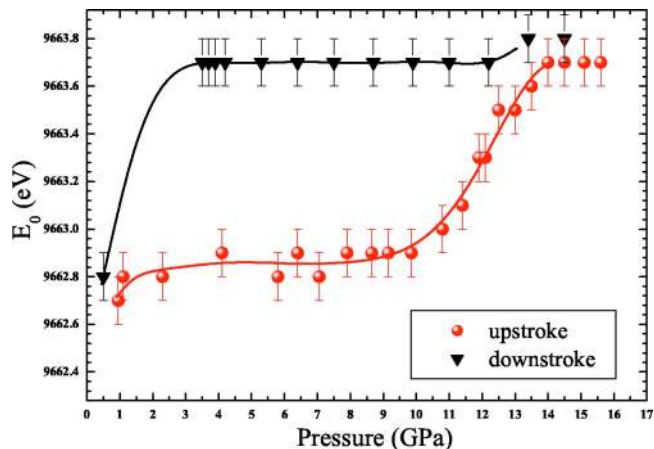


FIG. 12. Evolution of the Zn K -edge absorption onset (defined as the energy value corresponding to the maximum of the first derivative at the absorption edge) with pressures for the pressure upstroke (circle) and downstroke (triangle) spectra, respectively. The lines are a guide for the eye.

under pressure. All these results lead to the conclusion that neither a pretransitional effect nor a second-order isostructural phase transition would be observed in the wurtzite phase prior to the first-order transition to the rocksalt one.

Finally, it can be noticed that the elastic shear softening observed both experimentally⁷ and theoretically⁸ at room temperature (while c/a is measured to be constant) is in disagreement with the transition path proposed in Ref. 5. Actually, the weakening of C_{44} and C_{66} elastic moduli under pressure is probably due to bond-bending forces,⁴¹ in opposition to the proposed w -to- w' mechanism of transition where an initial decrease of the c/a ratio is expected before the opening of the bond-bending angles. Thus, the existence of a w -to- r transition path, as well as the nature of the intermediate phase, still remain open questions.

V. CONCLUSION

Combined energy-dispersive x-ray-diffraction and x-ray-absorption spectroscopy experiments have been used to determine the internal parameter u and the lattice parameters ratio c/a of the wurtzite phase as a function of pressure. In its experimental range of stability, the hexagonal wurtzite phase is shown to be undistorted by external hydrostatic pressures with no pretransitional effect, in good agreement with present *ab initio* calculations. While other zinc-based semiconductors can accurately be treated by freezing the zinc d electrons in the core, the present work shows that an accurate study of ZnO requires instead the explicit treatment of the d electrons of Zn as valence electrons. The simulations have also been performed above the experimental w -to- r phase transition. While the expected shift of the u value from 0.382 to 0.5 is observed, this transition is shown to be discontinuous in opposition to a possible displacive transformation.

ACKNOWLEDGMENTS

We are grateful to Alberta Congeduti for her help during the experiments at LURE. We thank E. Principi for his useful comments regarding the manuscript.

- *Electronic address: frederic.decremps@pmc.jussieu.fr
- ¹S. Baroni, P. Giannozzi, and A. Testa, Phys. Rev. Lett. **58**, 1861 (1987); P. Giannozzi, S. de Gironcoli, P. Pavone, and S. Baroni, Phys. Rev. B **43**, 7231 (1991).
 - ²V. Ozoliņš and A. Zunger, Phys. Rev. Lett. **82**, 767 (1999).
 - ³L. Bellaiche, K. Kunc, and J.M. Besson, Phys. Rev. B **54**, 8945 (1996).
 - ⁴J. Serrano, A. Rubio, E. Hernández, A. Muñoz, and A. Mujica, Phys. Rev. B **62**, 16 612 (2000).
 - ⁵S. Limpijumngong and W.R.L. Lambrecht, Phys. Rev. Lett. **86**, 91 (2001).
 - ⁶Surprisingly, this prediction seems to be in disagreement with Serrano *et al.* (Ref. 4) who found a GaN wurtzite phase stable (with respect to the w' structure) to about 200 GPa. To shed some light on that issue, we also performed the same type of calculation on w -GaN which appears to be stable versus w' —up to 500 GPa. However, Limpijumngong and Lambrecht (Ref. 5) do not give any quantitative data on the transition pressure, which could always be higher than 500 GPa.
 - ⁷F. Decremps, J. Zhang, B. Li, and R.C. Liebermann, Phys. Rev. B **63**, 224105 (2001).
 - ⁸A. Zaoui and W. Sekkal, Phys. Rev. B **66**, 174106 (2002).
 - ⁹F. Decremps, J. Pellicer-Porres, A.M. Saitta, J.-C. Chervin, and A. Polian, Phys. Rev. B **65**, 092101 (2002).
 - ¹⁰C.H. Bates, W.B. White, and R. Roy, Science **137**, 933 (1962).
 - ¹¹S. Desgreniers, Phys. Rev. B **58**, 14 102 (1998).
 - ¹²J.M. Recio, M.A. Blanco, V. Luaña, R. Pandey, L. Gerward, and J. Staun Olsen, Phys. Rev. B **58**, 8949 (1998).
 - ¹³H. Karzel, W. Potzel, M. Köferlein, W. Schiessl, U. Hiller, G.M. Kalvius, D.W. Mitchell, T.P. Das, P. Blaha, K. Schwartz, and M.P. Pasternak, Phys. Rev. B **53**, 11 425 (1996).
 - ¹⁴L. Gerward and J. Staun Olsen, J. Synchrotron Radiat. **2**, 233 (1995).
 - ¹⁵F. Decremps, J. Zhang, and R.C. Liebermann, Europhys. Lett. **51**, 268 (2000).
 - ¹⁶A. Filippini, J. Phys.: Condens. Matter **7**, 9343 (1995), and references therein.
 - ¹⁷The measurement of $a(P)$, $c(P)$ through XAFS is in fact less straightforward. XAFS is a measurement of the correlated interatomic distance. Thus, due to the positive contribution of vibrations perpendicular to the bond (σ_{\perp}^2), XAFS interatomic distances are expected to be slightly longer than XRD distances with a mismatch on the order of σ_{\perp}^2/R , decreasing with pressure (and increasing with temperature). It is not easy to correct the present results because the projection of vibration perpendicular to the bond direction is not known and should be measured independently. However, as a first approximation and within experimental errors, the vibrational effect can be neglected. A similar discussion could be found in A. Di Cicco, M. Taglienti, M. Minicucci, and A. Filippini, Phys. Rev. B **62**, 12 001 (2000), and references therein.
 - ¹⁸R. Letoullec, J.P. Pinceaux, and P. Loubeyre, High Press. Res. **1**, 77 (1988).
 - ¹⁹G.J. Piermarini, S. Block, J.D. Barnett, and R.A. Forman, J. Appl. Phys. **46**, 2774 (1975).
 - ²⁰H.K. Mao, J. Xu, and B.M. Bell, J. Geophys. Res. B **91**, 4673 (1986).
 - ²¹H. Tolentino, E. Dartyge, A. Fontaine, and G. Tourillon, J. Appl. Crystallogr. **21**, 15 (1988).
 - ²²M. Hagelstein, A. San Miguel, A. Fontaine, and J. Goulon, J. Phys. IV **7**, 303 (1997).
 - ²³S. Pascarelli, O. Mathon, and G. Aquilanti, *Proceedings of the ISSRNS Conference*, edited by Jaszowiec (Ustron, Warsovia, Poland, 2002).
 - ²⁴S. Baroni, A. Dal Corso, S. de Gironcoli, and P. Giannozzi, computer code PWSCF; <http://www.pwscf.org>
 - ²⁵N. Troullier and J.M. Martins, Phys. Rev. B **43**, 1991 (1993).
 - ²⁶K. Syassen, computer code DATLAB (Max Planck Institute, Stuttgart, Germany, 2003).
 - ²⁷A. Filippini and A. Di Cicco, Phys. Rev. B **52**, 15 135 (1995).
 - ²⁸A. Filippini and A. Di Cicco, Phys. Rev. B **51**, 12 322 (1995).
 - ²⁹A. Filippini and A. Di Cicco, Task Quarterly **4(4)**, 575 (2000), and references therein.
 - ³⁰A. Di Cicco, J. Phys. IV **7**, 171 (1997).
 - ³¹A. Mihelič, A. Kodre, I. Arčon, J. Padežnik Gomilšek, and M. Borowski, Nucl. Instrum. Methods Phys. Res. B **196**, 194 (2002).
 - ³²A. Di Cicco and F. Sperandini, Physica C **258**, 349 (1996).
 - ³³J. Padežnik Gomilšek, A. Kodre, I. Arčon, A.M. Loireau-Lozac'h, and S. Bénazeth, Phys. Rev. B **59**, 3078 (1999).
 - ³⁴A. Di Cicco, M. De Crescenzi, R. Bernardini, and G. Mancini, Phys. Rev. B **49**, 2226 (1994); A. Filippini, A. Di Cicco, P. Pianetta, and T. Kendelwicz, *ibid.* **53**, 15 571 (1996); V. Formoso, A. Filippini, A. Di Cicco, G. Chiarello, R. Felici, and A. Santaniello, *ibid.* **61**, 1871 (2000).
 - ³⁵A. Di Cicco, Phys. Rev. B **53**, 6174 (1996).
 - ³⁶A.L. Ankudinov, B. Ravel, J.J. Rehr, and S.D. Conradson, Phys. Rev. B **58**, 7565 (1998).
 - ³⁷J.E. Jaffe, J.A. Snyder, Z. Lin, and A.C. Hess, Phys. Rev. B **62**, 1660 (2000).
 - ³⁸J.Z. Jiang, J.S. Olsen, L. Gerward, D. Frost, D. Rubie, and J. Peyronneau, Europhys. Lett. **50**, 48 (2000).
 - ³⁹J.E. Jaffe and A.C. Hess, Phys. Rev. B **48**, 7903 (1993).
 - ⁴⁰A slight decrease can be seen in the $u(p)$ variation at pressure higher than 6 GPa (on the other hand, u is undoubtedly constant at lowest pressure). However, with respect to uncertainties, it is difficult to assume an occurrence of significant change in the intrinsic structural parameters of w -ZnO and we prefer to not jump to conclusion. On the other hand, it could be possible that we observe a precursor effect of the wurtzite-to-rocksalt transition. As a matter of fact, it is well known that the EXAFS technique, mostly sensitive to local order, may detect anomalies due to phase transition below the appearance of new x-ray-diffraction peaks. For example, it has been shown that EXAFS data on amorphous germanium can detect the crystallization before x-ray-diffraction: in the pressure domain where the transition takes place, the grains in the high-pressure form (crystal) are mostly nanosized and thus not detectable by x-ray diffraction. To come back to w -ZnO, it is interesting to see that toward about 9 GPa the appearance of new diffraction peaks reflects the wurtzite-to-rocksalt transition, while the corresponding equilibrium transition pressure is near 6 GPa at ambient temperature [see F. Decremps, J. Zhang, and R.C. Liebermann, Europhys. Lett. **51**, 268 (2000)].
 - ⁴¹P.N. Keating, Phys. Rev. **145**, 637 (1966).